Reactivity of *Pseudozyma antarctica* lipase B towards the Synthesis of End-capped Polycaprolactone for Drug Delivery

Pedro R. Figueiredo, Armando J.D. Silvestre, Andreia F. Sousa, and Alexandra T.P. Carvalho**

ABSTRACT. State-of-the-art delivery systems currently rely on chemical synthesis routes for drug encapsulation. However, these methods have inherent drawbacks concerning toxicity, selectivity, and the potential for burst release. To overcome these limitations, the enzymatic synthesis of polymer-drug conjugates emerges as a promising alternative to promote eco-friendliness and safety in production and grants precise control over the resulting structures. In this study, we delved into the reactivity of *Pseudozyma (Candida) antarctica* lipase B for polyesters' capping with small molecules. For that purpose, Quantum Mechanics/Molecular Mechanics simulations were used to predict the conjugation reactions. These predictions were translated to the laboratory, where the enzymatic reactions were replicated, subsequently benchmarking them against metal-catalysed reactions. The outcome of our experiments was the successful generation of end-capped oligo/polycaprolactone, with their molecular weights spanning from 540 to 2600 g mol^{-1} with an enzymatic approach, and slightly higher when applying conventional catalysis, and with isolation yields up to 68.4%. This work underscores the potential of enzyme-driven strategies in fabricating precisely engineered drug delivery systems, marking a significant stride toward more efficient and controlled therapeutics synthesis.

Keywords: CalB, QM/MM simulations, end-capping, enzymatic conjugation, ROP, bioresorbable polyesters; polycaprolactone; PCL

INTRODUCTION

Aliphatic polyesters, namely bioresorbable poly(ε-caprolactone) – PCL – and poly(glycolic acid) – PGA, have several biomedical applications e.g., in drug delivery systems and tissue engineering materials.[1–3] Their functionalization with bioactive molecules for *in vivo* release is highly relevant, as drug content can be easily controlled to expected ratios and it can help reduce cytotoxicity of the pristine drug when outside the targeted areas of interest.[4–6] The incorporation of small molecules is typically achieved by encapsulation, although with same limitations, namely the poor drug loading, potential of burst release, and, in some cases, also poor kinetic control over the drug release through time.[7] A growing and interesting alternative is the covalent bonding, as an end-group of the bioactive molecule to a polyester system, instead of just physical

interactions. In this case, the bonding of the drug could be calling up on its use as a ring-opening polymerization (ROP) initiator of, for example, PCL or PGA.[8] In these conjugates, polymers and drugs become covalently bonded, preventing off-target effects – which are especially negative for anticancer drugs – while also overcoming drug resistance. Depending on the polymer, polymer-drug conjugates (PDC) can reduce drug toxicity, increase the solubility, bio-availability, -compatibility and -degradability of the drugas well as an improved control of the delivery and release mechanism at the target sites.[9,10] Therefore, the tunability and predictability of the drug loading can be easily controlled, allied to the ability to incorporate hydrophilic molecules. More importantly, the release kinetics can be tuned without burst release.[11] In a previous work, we investigated the potential of PDCs for targeted cancer therapy. The *in situ* hydrolysis of thirty PDCs containing well-established anticancer drugs (e.g., SN38, doxorubicin, and paclitaxel) linked to biocompatible polyesters was evaluated. These PDCs are significantly important as they possess the potential to safely deliver bioactive molecules while minimizing side effects on healthy tissues.[12] Despite the interesting results achieved, the preparation of PDCs often requires harsh reaction conditions and metal catalysts (such as platinum and rhodium) are often used,[13,14] which are difficult to remove, making the products unsuitable for pharmaceutical applications and that could also lead to the degradation of unstable drugs.[15,16]

Enzyme-catalyzed ROP (eROP) is one of the most promising approaches to overcome the drawbacks of conventional chemical synthetic routes.[17,18] In general, enzymatic synthesis has several benefits, in particular: the use of milder/greener reaction conditions, high control of stereo-, chemo-, and regio-selectivity, and absence of toxic catalysts.[18,19] Particularly, the wildtype of serine hydrolases (e.g., esterases and lipases) have been extensively tested on eROP of lactones or macrocyclic esters.[20–28] The most commonly used enzyme in these reactions is the *Pseudozyma (Candida) antarctica* lipase B (CalB), a mesophilic enzyme that is normally immobilized on Lewatit VP OC 1600 (Novozyme 435).[29–32] For instance, Rychlicka and colleagues used it for the synthesis of *p*-methoxycinnamoylated phospholipids, while other groups produced prodrugs of nonsteroidal anti-inflammatory drugs.[33–35]

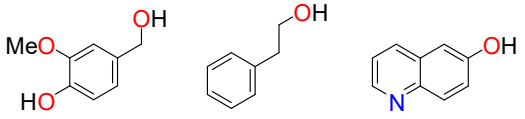

Figure 1. Structure of the considered capping agents: vanillyl alcohol, 2-phenylethanol, and 6-hydroxyquinoline.

Aiming to obtain an aromatic drug derivative-capped polyester, we started by studying the reactivity towards vanillyl alcohol (**VA**), 2-phenylethanol (**2PE**), and 6-hydroxyquinoline (**6HQ**) (Figure 1). **VA** exhibits remarkable antioxidant[36] and anti-inflammatory[37] properties, and studies suggest its use for the treatment of Parkinson's disease.[38] For **2PE**, potent antimicrobial

properties were identified.[39] **6HQ** serves as a starting heterocycle for pharmacological research. Its derivatives form a class of compounds with a wide range of biological activity. For example, ethyl 6-hydroxyquinoline-3-carboxylate derivatives have displayed excellent intracellular inhibitory activity towards the replication of hepatitis B Virus DNA.[40] However, to the best of our knowledge, their use and control release via end-capped polyesters is not described in the literature. Therefore, herein we describe the enzymatic conjugation of these compounds as initiators with polycaprolactone and polyethylene glycol by the widely used CalB enzyme. In this regard, we have characterized the full catalytic mechanism foremploying QM/MM simulations. These were later tested in the lab and benchmarked against a conventional polycondensation approach resorting to a metallic catalyst.

RESULTS AND DISCUSSION

in silico screening of macrocycle ring-opening polymerization

For the synthesis of end-capped oligomers, the *in silico* screening comprised, in the first step, the study of the ring-opening of two small macrocyclic esters commercially available – **ε-Cl** and glycolide. In all reactions (Scheme 1), the catalytic mechanism starts with a nucleophilic attack by the catalytic S105 which, in a concerted manner, transfers its proton to the H224 residue, forming the first tetrahedral intermediate (TI1). This is followed by proton rearrangement and ring-opening, which leads to the formation of the enzyme-activated monomer (EAM).

Scheme 1. General acylation mechanism for the CalB ring-opening of cyclic monomers.

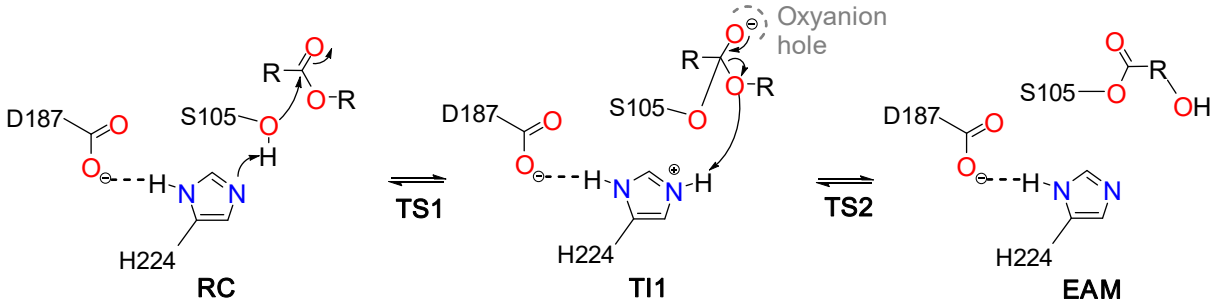

For the ring-opening reaction of **ε-Cl**, we observed that the active site arrangement promotes the leaving of the lactone oxygen atom (O_{lac}) as the Hε atom of H224 is closer to O_{lac} atom than the serine sidechain oxygen (O_{S105}).[41] The proton transfer is then facilitated for the lactone ring-opening (EAM formation). Here, we further explored the capacity of CalB to ring-opening glycolide in a first stage for conjugation with a capping agent in the deacylation step. The catalytic cycle starts with the entry of glycolide in the CalB active site (Figure 2A). During the approximation to S105, the substrate interacts with the oxyanion hole residues (Q106 and T40), Q157 through hydrogen bonds (HB), and the methylene group with V190 and I189 via Van der

Waals (VdW). These interactions were also recorded for **ε-Cl**.[41] The nucleophilic attack to generate the TI1 (Figure 2B) is associated with a $\Delta G^{\ddagger}$ of 15.7 kcal mol^{-1} (first transition state – TS1, Figure S1) and once this structure is formed (endergonic in relation to the reactants complex – RC**,** Figure S1), we observed a slight movement of the H224 residue. The receiving hydrogen interacts preferably with O_{S105} in an initial instant and then moves towards the O_{lac} where it stays for the reaction extension (1.8 Å for O_{lac} *vs.* 2.2 Å for O_{S105}, Figure 2A).

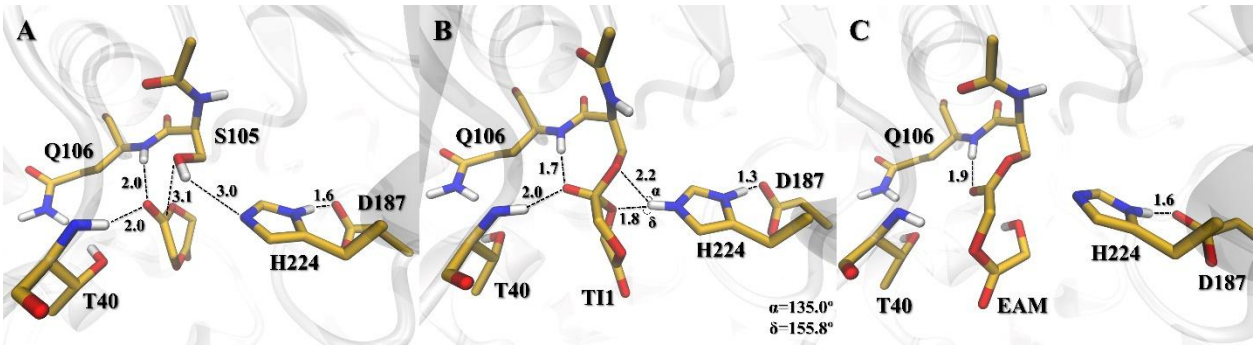

Figure 2. Active site pocket reference structures of the lowest energy stationary points RC, TI1, and EAM of glycolide (**A**, **B**, and **C**, respectively) where key distances are given in Å.

The forward reaction – ring-opening – is assisted by the Q157 sidechain that interacts with O_{lac} via HB. H224 performs the proton transfer and the C-O bond break to form the EAM structure (Figure 2C). For this reaction, we calculated a ΔG^{*} (TS2) of 26.3 kcal mol^{-1} that concerns the rate-determining step (rds) for the acylation part of the mechanism. The rds for the **ε-Cl** ring-opening reaction was also observed to be associated with the TS2 amounting to 9.8 kcal mol^{-1}, while the TS1 had a smaller calculated barrier of 8.8 kcal mol^{-1}.[41]

After analysis of the calculated energy barriers (Figure S1), both reactions for **ε-Cl** and glycolide ring-opening take place through a concerted ping-pong mechanism, meaning that proton transfer occurs simultaneously with the nucleophilic attack. The calculated barrier for ring-opening is considerably higher for glycolide when compared to **ε-Cl** (plus 16.5 kcal mol^{-1}, Figure S1). This difference can be attributed to the more hydrophilic nature of the substrate and its ring stability (6-membered) whereas in **ε-Cl**, the hydrophobic nature is more compatible with the active site residues and the 7-membered ring tension facilitates the C-O bond break.

The second part of the mechanism refers to the introduction of the initiator moiety (capping agent) to afford the capped-polyester conjugate that is released at the cycle's end for an increase in the polymer chain (Scheme 2). We have not tested the deacylation step of capping agents with a PGA model, since the glycolide ring-opening has a considerably higher barrier (Figure S1), hindering the formation of the EAM structure (Figure 2C).

Scheme 2. General deacylation step for the CalB enzymatic conjugation with capping agents (cap).

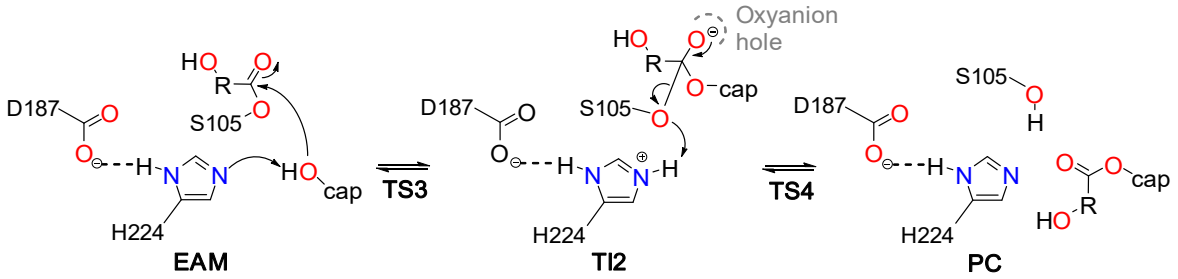

The capping agents in the active site (Figures 3A, D, and G) interact with hydrophobic residues belonging to the α10 helix (putative lid) namely L278, A281, and I285 that resemble a small hydrophobic pocket.According to the free energy profiles for these reactions (Figure 4), the formation of TI2 in the aliphatic initiators **VA** and **2PE**, is proposed to occur in a concerted mechanism (Figure 4). The associated transition state for these systems had a TS3 $\Delta G^{\ddagger}$ of about 20.0 kcal mol^{-1}, which evolved to TI2 as an exergonic reaction (in relation to RC). The formation of TI2 initiated by the **6HQ** is predicted to occur through a stepwise mechanism where proton transfer occurs in a first transition state (TS3^{a}) to generate an intermediate zwitterion system (I). The nucleophilic attack is associated with a second transition state (TS3^{b}) to form the TI2 structure. The associated ΔG for this reaction amounts to 27.2 kcal mol^{-1} (TS3^{a}, Figure 4). Comparing mechanisms for **6HQ**, the calculated barrier for the concerted mechanism predicts a 7.3 kcal mol^{-1} higher barrier (TS3, Figure 4) indicating the more affordable pathway of the stepwise mechanism. The unstable TI2 structure for this system is located at 13.7 kcal mol^{-1}.

At the TI2 (Figures 3B, E, and H), the substrates group interacts mostly with hydrophobic residues. In general, and in the tested alcohols (**VA**, **2PE**, and **6HQ**), the aromatic rings interact through VdW with the sidechain of I189, A281, and I285. For **6HQ** a T-shaped stacking was observed between W104 and the aromatic ring connected to the hydroxyl (Figure 1). In **VA** and **2PE** more hydrophobic interactions were found that may result in the higher stabilization of this stationary point (V154 and T40 in **VA**, and L278 and L535 for **2PE**). Concerning the polymeric unit, the PCL model also interacts mostly with hydrophobic residues, namely T138, V190, and I189, and the terminal hydroxyl function exhibits HB with the V134 carbonyl backbone (**6HQ**) or with the amide sidechain group of Q157 (**VA** and **2PE**) that are spatially close.

The $H\varepsilon_{H224}$ atom is closer to O_{init} than O_{S105} in all three cases (Figures 3B, E, and H) suggesting a higher energy barrier toward the forward reaction. This hydrogen bond is around 1.8 Å for O_{init}, and approximately 2.2 Å for O_{S105} in **VA** and **6HQ**. In **2PE**, the $H\varepsilon_{H224}$ atom is in a more centralized position between the two oxygen atoms (Figure 3H), which could help explain similar barriers for the formation of TS3 and TS4 (20.4 and 18.8 kcal mol^{-1}, Figure 4). The higher distance to O_{S105} in **VA** translates into a higher barrier for the PC formation and a 3.3 kcal mol^{-1} higher ΔG was observed over the backwards reaction (Figure 4). The instability of TI2 due

to the electronic structure of **6HQ** spawns a barrier of 34.5 kcal mol^{-1} and the reaction tends to evolve toward the reactants over the product formation, due to the more accessible energetic pathway. The formation of TS4 concerns the rds for the conjugation of **VA** and **6HQ** with the EAM structure, while similar values were calculated for the formation of TS3 and TS4 in the conjugation reaction of **2PE** (20.4 and 18.8 kcal mol^{-1}, respectively, Figure 4). These results predict the successful formation of end-capped PCL moieties with **VA** and **2PE** but a less feasible process for capping PCL with **6HQ**.

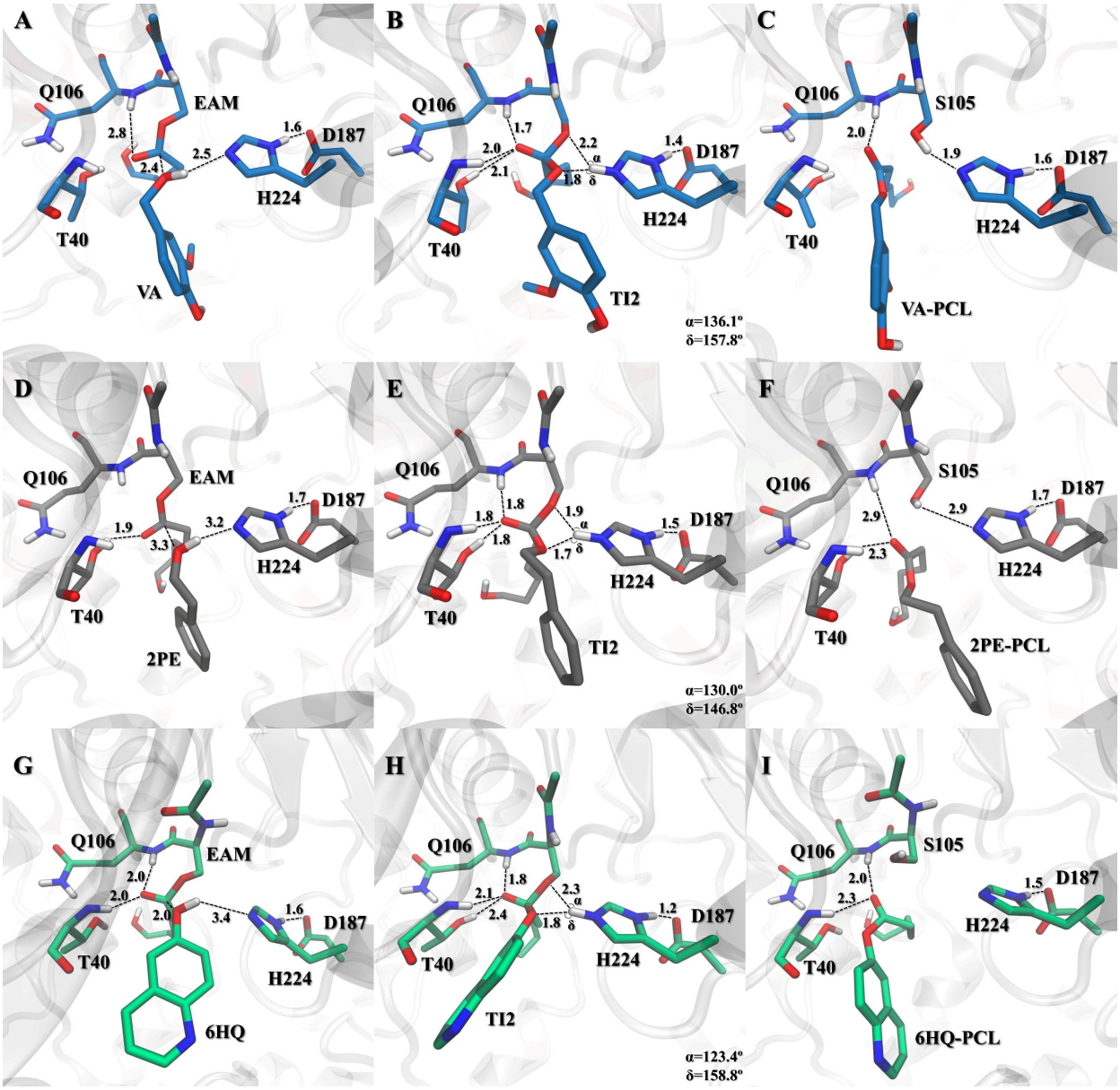

Figure 3. Active site pocket reference structures of the lowest energy stationary points EAM, TI2, and PC of end-capped PCL with **VA** (**A**, **B**, and **C**, respectively), **2PE** (**D**, **E**, and **F**, respectively), and **6HQ** (**G**, **H**, and **I**, respectively) where key distances are given in Å.

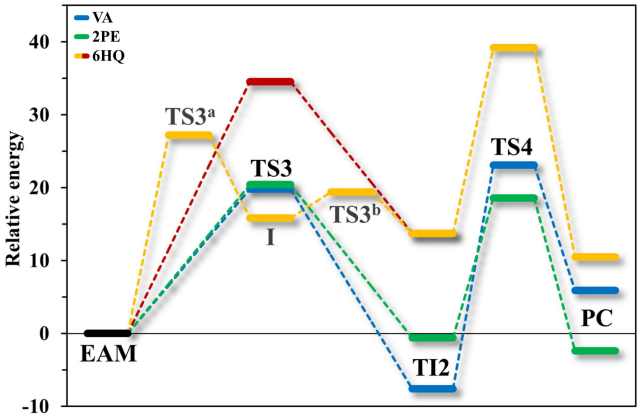

Figure 4. Free energy profiles for the initiator introduction step, derived from the FES. Relative barriers were calculated with B3LYP-D3/6-31++G(d,p)/parm99SB[42,43] and are given in kcal mol^{-1} for **VA**: $\Delta G^{\ddagger}$ TS3 (19.8), $\Delta G^{\ddagger}$ TS4 (23.1); **2PE**: $\Delta G^{\ddagger}$ TS3 (20.4), $\Delta G^{\ddagger}$ TS4 (18.8); and **6HQ**: $\Delta G^{\ddagger}$ TS3^{a} (27.2), ΔG^{*} TS3^{b} (19.4), $\Delta G^{\ddagger}$ TS3 (34.5), ΔG^{*} TS4 (39.2). The FES maps are supplied in supporting information (Figures S2-S4).

Experimental essays: synthesis of end-capped PCL oligomers

The enzymatic ROP of **ε-Cl** using the capping agents **VA**, **2PE**, and **6HQ** as initiators was studied. The successful conditions for the esterification of hexanoic acid according to Zieniuk *et al*,[44] were first applied (MTBE as solvent at 37 ºC for 24h) targeting an average molecular weight (M_n) of 2000-3000 g mol^{-1}.

Table 1. Reaction conditions used to generate end-capped products **VA-**, **2PE-**, and **6HQ-PCL**.

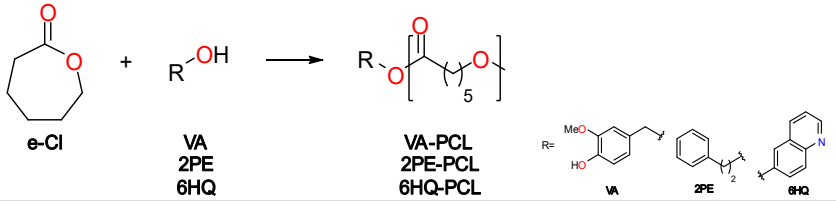

Entry	R-OH (eq)	Catalyst	Solvent	Temp (ºC)	Time (h)	Isolated product [a]
1	0.1 (**VA**)	N435	MTBE	37	24	**VA-PCL** M_n 2600 (6.0%) [b]
2	0.2 (**VA**)	N435	MTBE	37	24	**VA-PCL** M_n 1160 (44.6%) [c]
3	0.1 (**2PE**)	N435	MTBE	37	24	**2PE-PCL** M_n 1800 (58.8%)
4	0.1 (**6HQ**)	N435	MTBE	37	24	**PCL** M_n 3600 (53.7%)
5	0.02-0.37 (**6HQ**)	N435	Toluene	60-90	24	**PCL** M_n 7900 *ca.* (63.1%)
6	0.02 (**6HQ**)	N435	-	60	24	**PCL** M_n 5500 (18.7%)
7	0.1 (**VA**)	Sb_2O_3	-	170	3+18	**VA-PCL** M_n 3200 (68.4%)
8	0.1 (**2PE**)	Sb_2O_3	-	170	3+18	**2PE-PCL** M_n 2800 (52.0%)
9	0.1 (**6HQ**)	Sb_2O_3	-	170	3+18	**6HQ-PCL** M_n 2400 (67.0%)

[a] confirmed by ^{1}H NMR and M_n values assessed through ^{1}H NMR analysis (Figure S5), calculating the ratio between the integration area of the triplets assigned to adjacent -CH_2- group to the terminal hydroxyl and the repeating unit and given in g mol^{-1};[48,49] [b] Mother liquor has **VA** + **VA-PCL** M_n 900 (1:4.1, 39.2%); [c] Mother liquor has **VA** + **VA-PCL** M_n 900 (1:4.1, 39.2%).

Alcohols **VA** and **2PE** were able to initiate the enzymatic ring-opening polymerization reaction, affording the desired products (Table 1, entries 1-3). These were isolated with yields

ranging from 6.0 to 58.8% and M_n values between 1160-2600 g mol^{-1}, as targeted. In the reaction initiated by **6HQ** with the same conditions, only neat **PCL** was recovered as the reaction product (Table 1, entry 4). Further tests for a post-introduction of the **6HQ** initiator into **PCL** was also carried out. For that purpose, **PCL** ROP was initially optimized (results supplied in supporting information – Table S1) to afford oligomers (M_n ranging from 5500 to 7000 g mol^{-1}),[45–47] but **6HQ** was not incorporated (Table 1, entries 5-6).

For comparison reasons, in parallel, bulk ROP of **ε-Cl** with Sb_2O_3 catalyst was also carried out to synthesise the PCL end-capped products (Table 1, entries 7-9). These conditions allowed the desired products formation with yields higher than 52.0% and M_n values that ranged from 2400 to 3200 g mol^{-1}, nonetheless, a reaction high temperature was required (170 ºC).

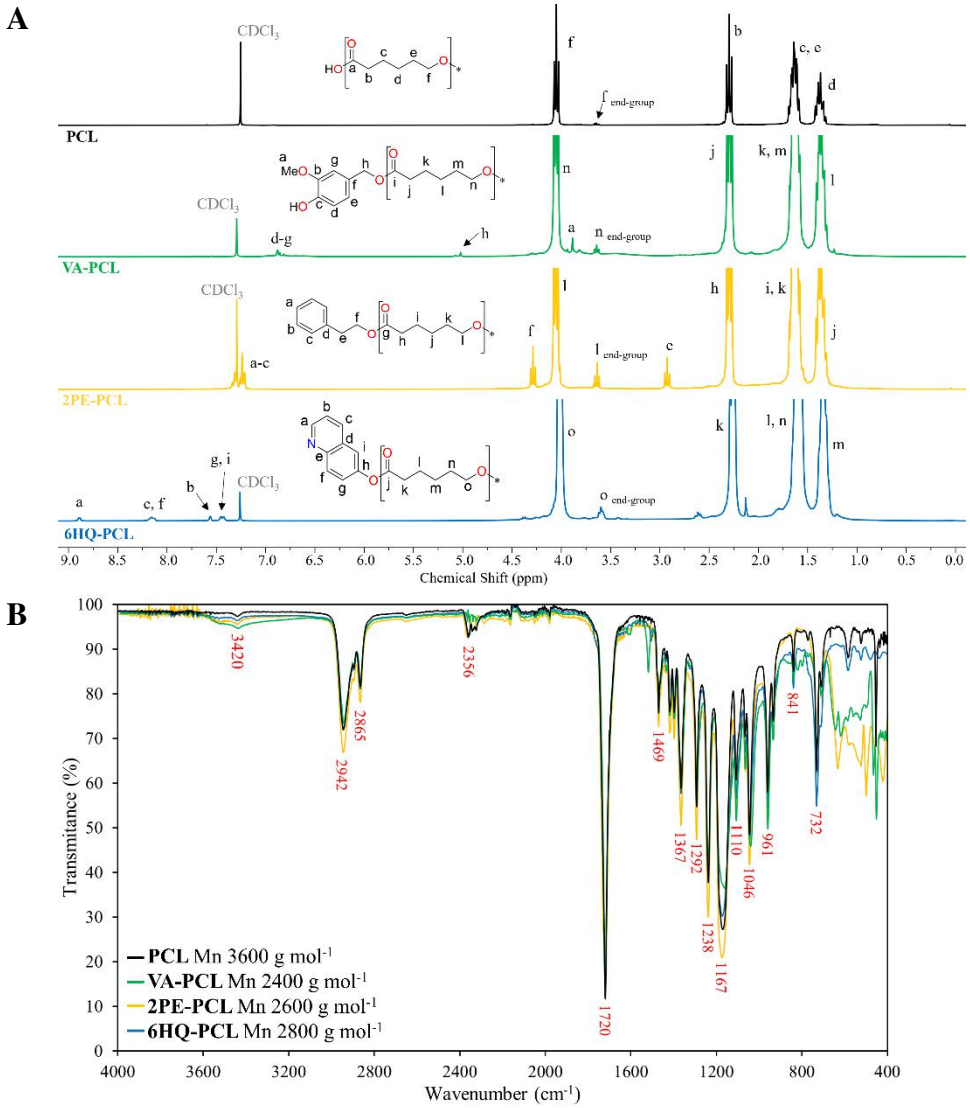

Figure 5. Stacked ^{1}H NMR spectra (**A**) and superimposed FTIR spectra (**B**) of **PCL** and end-capped **PCL** (**VA-**, **2PE-**, and **6HQ-PCL**). The ^{1}H and ^{13}C NMR and FTIR spectra are supplied in supporting information (Figures S5-S8).

The **PCL** and end-capped **PCL** structures were confirmed through FTIR and ^{1}H spectroscopy (Figure 5) as well as through ^{13}C NMR (Figure S5-S8). The ^{1}H NMR spectra of the end-capped products illustrate the main features of PCL, *viz*, a triplet at δ 3.99 ppm, assigned to the proton resonance of the repeating -CH_2- groups and the -CH_2- group near the terminal hydroxyl at δ 3.58 ppm.[49] The -CH_2- group adjacent to the ester function appears as a triplet signal at around δ 2.24 ppm, while the remaining -CH_2- groups appear as two multiplets at δ 1.58 and 1.31 ppm. Importantly the -CH_2- group from the capping molecule adjacent to the PCL chain appears as a small singlet resonance at δ 5.02 ppm for **VA-PCL** and as a triplet at δ 4.26 ppm for **2PE-PCL**. In the case of **6HQ-PCL**, H_i and H_g resonances appear as two singlets at δ 7.43 and 7.46 ppm (Figure 5A). In the ^{13}C NMR spectra, the distinctive characteristics of the PCL chain are observed (except for product **2PE-PCL**, which exhibits three additional signals around δ 127.00 ppm, attributed to the aromatic protons). Notably, these distinctive features include a signal at approximately δ 64.20 ppm, corresponding to the carbon in the repeating **-**CH_2**-** groups, another at δ 62.70 ppm for the **-**CH_2**-** group near the terminal hydroxyl, and a peak at δ 173.70 ppm indicative of the carbonyl group.

The characteristic **PCL** vibration bands[50] were observed in the FTIR spectra of the end-capped oligomers since the major portion of these moieties is comprise the repeating units of PCL, namely: the asymmetric/symmetric stretching bands of **-**CH_2**-** at 2942 and 2865 cm^{-1}, respectively, and one intense and sharp vibrational band at 1720 cm^{-1} ascribed to the C=O stretching of the ester group. Another two high-intensity peaks arise at 1238 and 1167 cm^{-1} concerning the asymmetric and symmetric stretching mode of C-O-C from the ester group. In addition, the broadband centred at 3420 cm^{-1} shows the O-H stretching of the terminal hydroxyl group and, in the case of **VA-PCL**, the stretching of the aromatic hydroxyl from the vanillin portion is also detected (from Table 1 – **PCL**: entry 4, **VA-PCL**: entry 1, **2PE-PCL**: entry 8, and **6HQ-PCL**: entry 9). These attributions are in agreement with the reported values for similar oligomers.[50–52]

The incorporation rates (proportion of capping agent incorporated into the total mass of PCL) of the capping molecules (**VA**, **2PE**, and **6HQ**) into PCL vary significantly between the tested enzymatic and conventional synthesis (estimated through ^{1}H NMR analysis, calculating the ratio between the integration area of the resonance assigned to the **-**CH_2**-** group adjacent to the terminal hydroxyl group and a specific resonance of the capping unit, namely the signal attributed to H_h and H_f for **VA** and **2PE**, respectively, and H_i for **6HQ**, Figure 5A). In the enzymatic synthesis, **VA** and **2PE** demonstrate high incorporation rates of 64% and 86%, respectively. In contrast, the conventional synthesis yields lower incorporation rates, with **VA** at 20%, **2PE** at 59%, and **6HQ** at 24%. This comparative analysis highlights the more efficient

pathway (enzymatic) in achieving higher capping incorporation rates in PCL, despite the fact that a lower amount of final product was isolated.

Thermal analysis

The impact of end-capping on the properties of PCL was assessed using thermal analysis techniques. We compare the properties of **PCL** (Table S1, entry 2) with those of the end-capped PCL products (Table 1 entries 7-9). The latter revealed thermal characteristics equivalent to neat PCL (namely thermal stability and melting temperature), which are a promising aspect for their practical application.

Table 2. Onset of decomposition (T_{on}), maximum decomposition ($T_{d,max}$), glass transition (T_g), and melting (T_m), temperatures and enthalpy (ΔH) of **PCL** and end-capped PCL.

Sample	TGA		DMTA	DSC	
	$T_{on,5\%}$ (°C)	$T_{d,max}$ (°C)	T_g (°C)	T_m (°C)	ΔH (J g^{-1})
PCL	305	405	-28.5	56.2	76.4
VA-PCL	315	391	-0.6	50.6	74.2
2PE-PCL	289	303; 387	-41.2	43.5	74.8
6HQ-PCL	313	401	-11.7	53.0	80.2

In terms of thermal stability (Table 2 and Figure S9), the conjugated PCL revealed a decomposition temperature at 5% weight loss between 289-315 °C, also in line with the same parameter for **PCL**. The same trend was also observed for the maximum decomposition temperature. For product **2PE-PCL**, the maximum decomposition temperature at 387 °C has a shoulder around 303 °C.

PCL and its corresponding capped counterparts were also characterised using DMTA, and the corresponding thermograms are presented in Figure S10. The results revealed differences in the T_g values for the end-capped PCL when compared to neat **PCL** (Table 2). Notably, the highest change (+27.9 °C) in T_g was observed for the end-capped product **VA-PCL**, suggesting a modification in the molecular mobility of the polymeric matrix and in line with a less flexible moiety with the aromatic group capping.

The DSC thermograms (Figure S11) showed that the end-capped oligomers show only a slight reduction (up to 12.7 °C, Table 2) in the T_m compared to **PCL** (56.2 °C). Additionally, the enthalpy changes (ΔH) during the melting process for the tested end-capped compounds were similar to that of **PCL** (approximately 76.4 J g^{-1}) with negligible variations of up to 3.8 J g^{-1} (Table 2 and Figure S11). This suggests that the incorporation of the tested capping molecules in PCL resulted in minimal changes in the energy required for phase transitions, indicating a similarity in their thermal behaviour when compared to pure PCL.

CONCLUSIONS

In this work, we have tested the CalB-mediated ring-opening reaction of the glycolide. The calculated barrier for this reaction amounts to 26.3 kcal mol^{-1} showing that this process is slow with this enzyme. In the second stage (formation of the end-capped PCL model), the reaction initiated by **VA** and **2PE** was predicted to have a ΔG below 23.1 kcal mol^{-1} attesting the possibility of product formation. In the case of **6HQ**, the formation of the TI2 was proposed to take place through a stepwise mechanism as the concerted mechanism has a calculated 7.3 kcal mol^{-1} higher barrier than the other mechanism (Figure 4). However, the unstable TI2 resulted in a rds of 39.2 kcal mol^{-1} for the formation of the TS4, and the process was considered less feasible. We attribute the stability of the phenoxide ion (generated from **6HQ**) and the fact that it is a good leaving group to the impossibility of generating the desired product.

The polymerization reactions underwent experimental testing, and in line with the *in silico* predictions, the capped products **VA-PCL** and **2PE-PCL** exhibited a feasible pathway for their synthesis using CalB as catalyst. Contrarily, an enzymatic approach (with CalB) proved impractical to generate the **6HQ-PCL** product, which is in accordance with the *in silico* predictions. However, this product was successfully synthesized by employing Sb_2O_3 as catalyst and drastically higher temperatures.

When compared to the enzymatic reactions (Table 1), **VA-PCL** and **2PE-PCL** were isolated with higher M_n when the metallic catalyst was employed (2600 *vs.* 3200 g mol^{-1} for **VA-PCL**, and 1800 *vs.* 2800 g mol^{-1} for **2PE-PCL**). Concerning the isolation yields, similar values were achieved for the synthesis of **2PE-PCL** but, in **VA-PCL**, the metallic catalyst allowed the formation of higher M_n that were capable of easily precipitating from the solution resulting in more than 62% yield increase over the enzymatic catalyst.

The thermal analysis showed that the thermal stability and melting temperature of the synthesized end-capped PCL are equivalent to those of neat **PCL**. The notable divergence among these oligomers lies in their T_g, which in all cases, is below the physiological temperature of 37 ºC. Therefore, these results suggest that the studied end-capped oligomers have potential applications in drug delivery, similar to those of PCL conjugated with active compounds.

METHODS

Initial setup

The initial structure was modelled from the *Pseudozyma (Candida) antarctica* lipase B (PDB ID 5A71, homodimer with 0.91 Å resolution)[53] crystal structure. The protonation states were assigned with MolProbity[54] and confirmed through visual inspection. The TI1 and TI2 residues were geometry optimized in Gaussian09[55] using B3LYP[42] with the 6-31G(d,p) basis set in the

gas phase. The atomic partial charges were calculated resorting to the Restrained Electrostatic Potential (RESP) methodology.[56] The initial position of the tetrahedral structures was obtained by the flexible side-chain covalent docking method[57] and performed with the AutoDock4.2 suite of programs using the Lamarckian Genetic Algorithm (LGA).[58] A total of 150 runs were carried out. The population was set to 300, the maximum number of generations 27000, and the maximum number of energy evaluations 2500000.

Molecular dynamics

The MD simulations were performed using the Amber molecular dynamics program (AMBER18)[59] with the ff14SB[60] force field. The structures were placed within a pre-equilibrated orthorhombic box of MTBE and two sodium ions were added to neutralize each system. The ParmEd utility of AmberTools[59] was used to add the Lennard-Jones parameters. An initial energy minimization and 100 ps of heating and density equilibrations were carried out using Langevin dynamics with small restraints of 10.0 kcal mol^{-1} on the protein. The systems were then left to equilibrate without any restraint for 2 ns in an NVT ensemble. 5 ns of production simulations were then performed at 318.15 K in an NPT ensemble using the Langevin dynamics with a collision frequency of 1 ps^{-1}. Constant pressure periodic boundary conditions were imposed with an average pressure of 1 atm. Isotropic position scaling was used to maintain pressure with a relaxation time of 2 ps and the time step was set to 2 fs. SHAKE constraints were applied to all bonds involving hydrogen atoms.[61] The electrostatic interactions were calculated resorting to the Particle Mesh Ewald (PME) method[62] with a cut-off distance of 10.0 Å.

Quantum mechanics/molecular mechanics calculations

The QM/MM Umbrella Sampling calculations[63–65] were performed using the internal semi-empirical hybrid QM/MM functionality implemented in AMBER18[59] with periodic boundary conditions. The last MD reference structure of each complex was used as the initial structure for the QM/MM calculations. The PM3 semi-empirical method[66,67] was employed to describe the QM region, while the MM region was described by the Amber ff14SB force field.[60] Reactions were conducted at the enzyme's optimal temperature (318.15 K). Electrostatic embedding[68] was employed and the boundary was treated via the link atom approach. Long-range electrostatic interactions were described by an adapted implementation of the PME method for QM/MM.[69] A set of descriptors (collective variables) was chosen for the free energy surface sampling, which would be able to characterize all the states of the simulated systems (Figure 6). We have employed the distances d_1 and d_4 representing the proton transfer to and from H224, and d_2 and d_3 corresponding to the C–O bond forming and breaking.

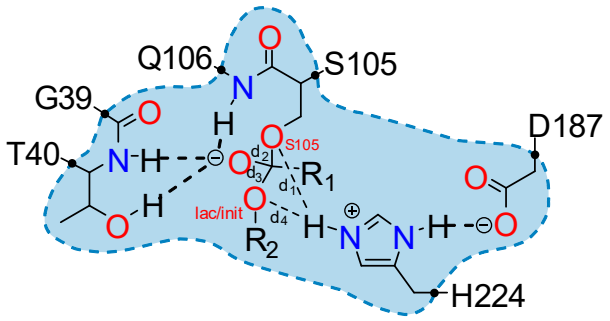

Figure 6. Defined QM region (atoms inside the shaded zone). Quantum link atoms are indicated as black dots. TI1 R_1,R_2=cyclic monomer and TI2 R_1=polymer chain, R_2=initiator residue (O_{lac} is applied to TI1 and O_{init} to TI2). The fully defined QM region is supplied in Figure S12.

To keep the collective variables at the requested distances and to ensure enough overlap between windows, an umbrella constraint force of 200 kJ mol^{-1} A^{-2} was used along the reaction path and incrementally increased to 1000 kJ mol^{-1} A^{-2} as the reaction coordinates deflect from the minimum energy path. For every window, a total of 25 ps was simulated with a time step of 1 fs and the distances scanned from 1.0 to 2.0 Å (d_1 and d_4, Figure 6), and from 1.4 to 2.5 Å (d_2 and d_3, Figure 6) in 0.1 Å steps, comprising a total of 132 simulations per step. The free energy profiles were obtained by combining all the statistics from each reaction simulation by resorting to WHAM with the Monte Carlo bootstrap error analysis.[70,71] The minimum energy path was traced with the MEPSA software v1.4[72] and all the averaged minima structures were retrieved and optimized with PM6/ff14SB to make all the figures.

Density functional theory corrections

For the high-level layer corrections, we resorted to a method described in reference 73, which is based on the work of Truhlar and co-workers.[74,75] This method compensates for the limitations of semi-empirical methods. Multiple structures of the QM region (with H link atoms) were extracted and submitted to single-point energy calculations in the gas phase. Structures were extracted from the whole Potential of Mean Force. The calculations were carried out in ORCA software v5.0.1,[76] with the semi-empirical PM3[66,67] and B3LYP-D3/6-31++G(d,p).[42,43] The corrected energy term (E_{corr}) was interpolated from those structures employing equation (1):

$$E_{corr} = E_{MM}^{PM3} + S(\Delta E_{PM3}^{B3LYP}) \quad (1)$$

where the term ΔE_{PM3}^{B3LYP} corresponds to the difference between the free energy for the high-level layer set, calculated with B3LYP-D3/6-31++G(d,p)[42,43] and PM3,[66,67] while S represents the cubic spline function of the difference between the high-level and low-level theories representing the QM region.

Materials

2-Phenylethanol (99.0%), 6-hydroxyquinoline (95.0%), hexanoic acid (99.5%), lipase immobilized from *Candida antarctica*, ε-caprolactone (97.0%), and molecular sieves 3 Å were acquired from Sigma–Aldrich (Oeiras, Portugal). Antimony trioxide (99.0%) was purchased from Fluka (Oiras, Portugal). Sodium bicarbonate (99.0+%) was obtained from Fisher Scientific (Porto Salvo, Portugal). Vanillyl alcohol (99.0%) was supplied by ACROS Organics (Porto Salvo, Portugal). All solvents were analytical grade or higher and used as received without further purification. Reactions were performed in a VWR VMS-C7 Advanced, at different temperatures with magnetic stirring between 500-1500 RPM.

^{1}H and ^{13}C NMR spectroscopy

The ^{1}H and ^{13}C NMR analyses of samples dissolved in $CDCl_3$-d were collected in a Bruker AMX 300 spectrometer (Wissem-bourg, France) operating at 300 or 75 MHz. The chemical shifts were expressed in ppm and the coupling constants in Hz. The $CDCl_3$-d signal was used as reference set at 7.26 and 77.2 ppm for ^{1}H NMR and ^{13}C NMR, respectively. MestReNova v14.2.1 was used to support ^{1}H and ^{13}C NMR spectra interpretation.

FTIR spectroscopy

The infrared spectra were collected in a spectrometer PARAGON 1000 FTIR spectrometer equipped with a single-horizontal Golden Gate ATR cell (Perkin-Elmer, MA, United States). The spectra were recorded after 128 scans, at a resolution of 4 cm^{-1}, within the range of 400 to 4000 cm^{-1}.

Thermal analysis

TGA was performed in a Shimadzu TGA50 analyzer equipped with a platinum cell with platinum pans to encapsulate the samples. The thermograms were recorded under a nitrogen flow (20 mL min^{-1}) and heated at a constant heating rate of 10 °C min^{-1} from room temperature up to 800 °C. DSC thermograms were obtained with a Pyris Diamond DSC calorimeter from Perkin Elmer (Waltham, MA, USA). Scans were carried out at a 10 °C min^{-1} heating rate and the temperature ranged from -90 °C to 120 °C. Two heating/cooling cycles were performed. The first heating scan was carried out to erase the thermal history of the polymers and the second heating was performed after a rapid cooling from the melted polymer. The DMTA of thick samples (10.0×5.0×1.0 mm^3), placed in a foldable stainless-steel materials pocket of Triton technology, was performed with a Tritec 2000 DMTA Triton equipment (WA, USA) operating in the single cantilever bending geometry. Tests were carried out in multifrequency mode (1 and 10 Hz), from −100 to 120 °C, at 2 °C min^{-1}. The glass-transition temperature of end-capped compounds was determined from the maximum Tan δ *vs.* temperature curve, at 1 Hz.

Synthetic procedures for end-capping PCL

CalB-assisted ROP: **ε-Cl** (10 eq), CalB (5%w), and molecular sieves 3 Å were mixed in MTBE (1 mL) with the capping agents (**VA**, **2PE**, or **6HQ**), and heated at 37 °C for 24 h. At the end of the reaction, 5 mL of acetone was then added, and the enzyme and molecular sieves removed by filtration. The mother liquor was concentrated under reduced pressure. The resulting oil was dropwise added to 20 mL of cold methanol where a white solid precipitated. This was filtered, washed with cold methanol, and left to dry in a 40 °C oven overnight. The recovered white solid was identified as the corresponding end-capped product (**VA-PCL** or **2PE-PCL**).

Metal-catalysed ROP: A suspension of **VA**, **2PE**, or **6HQ**, **ε-Cl** (10 eq), and Sb_2O_3 (1 mol%) was gradually heated from 80 °C to 170 °C during 3 h. Then, the mixture was left at 170 °C for 18 h, under a nitrogen atmosphere. In the end of the reaction, 50 mL of cold methanol was added, and the flask placed in the ultrasounds for 20 min. The suspension was filtered and washed with cold methanol before being kept overnight in a 40 °C oven to dry. The isolated solid was identified as the corresponding end-capped product (**VA-PCL**, **2PE-PCL**, or **6HQ-PCL**).

The ^{1}H, ^{13}C NMR and FTIR spectra are supplied in Figures S5-S8.

ASSOCIATED CONTENT

Supporting Information

The Supporting Information is available free of charge on the ACS Publications website at DOI: Calculated free energy surfaces (Figures S1-S4); ^{1}H, ^{13}C NMR and FTIR spectra of **PCL** and end-capped products (Figures S5-S8); TGA, DMTA, and DSC heating thermograms (Figures S9-S11); Representation of the complete QM region (Figure S12); Synthesis of **PCL**.

AUTHOR INFORMATION

Authors

Pedro R. Figueiredo – Center for Neuroscience and Cell Biology (CNC), Institute for Interdisciplinary Research (IIIUC), University of Coimbra, 3004-504 Coimbra, Portugal; PhD Programme in Experimental Biology and Biomedicine, Institute for Interdisciplinary Research (IIIUC), University of Coimbra, Casa Costa Alemão, 3030-789 Coimbra, Portugal; orcid.org/0000-0002-1243-0265; pmrfigueiredo@cnc.uc.pt

Armando J.D. Silvestre – CICECO – Aveiro Institute of Materials, Department of Chemistry, University of Aveiro, 3810-193 Aveiro, Portugal; orcid.org/ 0000-0001-5403-8416; armsil@ua.pt

Corresponding Authors

Andreia F. Sousa – CICECO – Aveiro Institute of Materials, Department of Chemistry, University of Aveiro, 3810-193 Aveiro, Portugal; Centre for Mechanical Engineering, Materials and Processes, Department of Chemical Engineering, University of Coimbra, Rua Sílvio Lima – Polo II 3030-790 Coimbra, Portugal; orcid.org/ 0000-0003-3044-3016; andreiafs@ua.pt

Alexandra T.P. Carvalho – Center for Neuroscience and Cell Biology (CNC), Institute for Interdisciplinary Research (IIIUC), University of Coimbra, 3004-504 Coimbra, Portugal; Almac Sciences, Department of Biocatalysis and Isotope Chemistry, Almac House, 20 Seagoe Industrial Estate, Craigavon, BT63 5QD, Northern Ireland, United Kingdom; orcid.org/0000-0003-2827-5527; atpcarvalho@uc.pt

Author Contributions

PRF investigation, image conceptualization, formal analysis, results interpretation, and manuscript writing. **AJDS** validation, research supervision, and manuscript writing. **AFS** conceptualization, funding acquisition, formal analysis, results interpretation, validation, research supervision, and manuscript writing. **ATPC** formal analysis, results interpretation, validation, research supervision, and manuscript writing.

Notes

The authors declare no competing financial interest.

ACKNOWLEDGMENTS

This work was sponsored through: grants SFRH/BD/144303/2019, CEECIND/02322/2020, and IF/01272/2015; AFS acknowledge FCT for the research contract CEECIND/02322/2020 (DOI 10.54499/2020.02322.CEECIND/CP1589/CT0008); and projects CNC – Center for Neurosciences and Cell Biology UIDB/04539/2020 and CICECO – Aveiro Institute of Materials UIDB/50011/2020, UIDP/50011/2020 & LA/P/0006/2020, financed by Portuguese National funds via FCT – Foundation for Science and Technology, Regional Operational Program (CENTRO2020) under the Portuguese Partnership Agreement 2020 by the European Regional Development Fund (ERDF), and FCT/MCTES (PIDDAC).

The authors acknowledge the computing resources made available by the Laboratory for Advanced Computing of the University of Coimbra (LCA-UC) funded by FCT and FEDER under the Advanced Computing Project CPCA/A1/447491/2021.

REFERENCES

(1) Cameron, D. J. A.; Shaver, M. P. Aliphatic Polyester Polymer Stars: Synthesis, Properties and Applications in Biomedicine and Nanotechnology. *Chem. Soc. Rev.* **2011**, *40* (3), 1761–1776. doi.org/10.1039/C0CS00091D.

(2) Hutanu, D.; Frishberg, M. D.; Guo, L.; Darie, C. C. Recent Applications of Polyethylene Glycols (PEGs) and PEG Derivatives. *Modern Chemistry & Applications* **2014**, *2* (2), 1–6. doi.org/10.4172/2329-6798.1000132.

(3) Grossen, P.; Witzigmann, D.; Sieber, S.; Huwyler, J. PEG-PCL-Based Nanomedicines: A Biodegradable Drug Delivery System and Its Application. *J. Control. Release* **2017**, *260*, 46–60. doi.org/10.1016/j.jconrel.2017.05.028.

(4) Luo, S.-H.; Wu, Y.-C.; Cao, L.; Wang, Q.-F.; Chen, S.-X.; Hao, Z.-F.; Jing, L.; Wang, Z.-Y. One-Pot Preparation of Polylactic Acid-Ibuprofen Conjugates and Their Performance Characterization. *Polym. Chem.* **2017**, *8* (45), 7009–7016. doi.org/10.1039/C7PY01213F.

(5) Saiyad, M.; Shah, N. Nanopolymers in Drug Delivery System. *Materials Today: Proceedings* **2022**, *67*, 25–30. doi.org/doi.org/10.1016/j.matpr.2022.05.019.

(6) Singh, B.; Singh, S.; Gautam, A.; Sutherland, A.; Pal, K. Preparation and Characterization of PLA Microspheres as Drug Delivery System for Controlled Release of Cetirizine with Carbon Dots as Drug Carrier. *Polym. Bull.* **2022**. doi.org/10.1007/s00289-022-04331-x.

(7) Trivedi, R.; Kompella, U. B. Nanomicellar Formulations for Sustained Drug Delivery: Strategies and Underlying Principles. *Nanomedicine* **2010**, *5* (3), 485–505. doi.org/10.2217/nnm.10.10.

(8) Phan, H.; Kortsen, K.; Englezou, G.; Couturaud, B.; Nedoma, A. J.; Pearce, A. K.; Taresco, V. Functional Initiators for the Ring‐opening Polymerization of Polyesters and Polycarbonates: An Overview. *Journal of Polymer Science* **2020**, *58* (14), 1911–1923. doi.org/10.1002/pol.20200313.

(9) Bilia, A. R.; Isacchi, B.; Righeschi, C.; Guccione, C.; Bergonzi, M. C. Flavonoids Loaded in Nanocarriers: An Opportunity to Increase Oral Bioavailability and Bioefficacy. *FNS* **2014**, *05* (13), 1212–1327. doi.org/10.4236/fns.2014.513132.

(10) Liu, Y.; Khan, A. R.; Du, X.; Zhai, Y.; Tan, H.; Zhai, G. Progress in the Polymer-Paclitaxel Conjugate. *Journal of Drug Delivery Science and Technology* **2019**, *54*, 101237. doi.org/10.1016/j.jddst.2019.101237.

(11) Manandhar, S.; Sjöholm, E.; Bobacka, J.; Rosenholm, J. M.; Bansal, K. K. Polymer-Drug Conjugates as Nanotheranostic Agents. *JNT* **2021**, *2* (1), 63–81. doi.org/10.3390/jnt2010005.

(12) Figueiredo, P. R.; González, R. D.; Carvalho, A. T. P. Insights in the Degradation of Polymer-Drug Conjugates by an Overexpressed Enzyme in Cancer Cells. *J. Med. Chem.* **2023**.

(13) *Handbook of Polymers for Pharmaceutical Technologies. Volume 3. Biodegradable Polymers*; Thakur, V. K., Thakur, M. K., Eds.; Scrivener Publishing: Beverly, MA, 2015.

(14) Sharma, R.; Singla, N.; Mehta, S.; Gaba, T.; Rawal, R.; Rao, H. S.; Bhardwaj, T. R. Recent Advances in Polymer Drug Conjugates. *MRMC* **2015**, *15* (9), 751–761. doi.org/10.2174/1389557515666150519104507.

(15) Tong, R.; Cheng, J. Drug-Initiated, Controlled Ring-Opening Polymerization for the Synthesis of Polymer–Drug Conjugates. *Macromolecules* **2012**, *45* (5), 2225–2232. doi.org/10.1021/ma202581d.

(16) Yin, Q.; Tong, R.; Xu, Y.; Baek, K.; Dobrucki, L. W.; Fan, T. M.; Cheng, J. Drug-Initiated Ring-Opening Polymerization of *O* -Carboxyanhydrides for the Preparation of Anticancer Drug–Poly(*O* -Carboxyanhydride) Nanoconjugates. *Biomacromolecules* **2013**, *14* (3), 920–929. doi.org/10.1021/bm301999c.

(17) Jérôme, C.; Lecomte, P. Recent Advances in the Synthesis of Aliphatic Polyesters by Ring-Opening Polymerization. *Adv. Drug Deliv. Rev.* **2008**, *60* (9), 1056–1076. doi.org/10.1016/j.addr.2008.02.008.

(18) Zhang, J.; Shi, H.; Wu, D.; Xing, Z.; Zhang, A.; Yang, Y.; Li, Q. Recent Developments in Lipase-Catalyzed Synthesis of Polymeric Materials. *Process Biochemistry* **2014**, *49* (5), 797–806. doi.org/10.1016/j.procbio.2014.02.006.

(19) Kadokawa, J.; Kobayashi, S. Polymer Synthesis by Enzymatic Catalysis. *Curr Opin Chem Biol* **2010**, *14* (2), 145–153. doi.org/10.1016/j.cbpa.2009.11.020.

(20) Uyama, H.; Kobayashi, S. Enzymatic Ring-Opening Polymerization of Lactones Catalyzed by Lipase. *Chem. Lett.* **1993**, *22* (7), 1149–1150. doi.org/10.1246/cl.1993.1149.

(21) He, F.; Li, S.; Vert, M.; Zhuo, R. Enzyme-Catalyzed Polymerization and Degradation of Copolymers Prepared from ϵ-Caprolactone and Poly(Ethylene Glycol). *Polymer* **2003**, *44* (18), 5145–5151. doi.org/10.1016/S0032-3861(03)00562-7.

(22) Albertsson, A.-C.; Srivastava, R. K. Recent Developments in Enzyme-Catalyzed Ring-Opening Polymerization. *Advanced Drug Delivery Reviews* **2008**, *60* (9), 1077–1093. doi.org/10.1016/j.addr.2008.02.007.

(23) Yang, Y.; Yu, Y.; Zhang, Y.; Liu, C.; Shi, W.; Li, Q. Lipase/Esterase-Catalyzed Ring-Opening Polymerization: A Green Polyester Synthesis Technique. *Process Biochemistry* **2011**, *46* (10), 1900–1908. doi.org/10.1016/j.procbio.2011.07.016.
(24) Huang, Y.; Li, L.; Li, G. An Enzyme-Catalysed Access to Amphiphilic Triblock Copolymer of PCL-b-PEG-b-PCL: Synthesis, Characterization and Self-Assembly Properties. *Designed Monomers and Polymers* **2015**, *18* (8), 799–806. doi.org/10.1080/15685551.2015.1078113.
(25) Kobayashi, S. Enzymatic Ring-Opening Polymerization and Polycondensation for the Green Synthesis of Polyesters. *Polymers for Advanced Technologies* **2015**, *26* (7), 677–686. doi.org/10.1002/pat.3564.
(26) Shoda, S.; Uyama, H.; Kadokawa, J.; Kimura, S.; Kobayashi, S. Enzymes as Green Catalysts for Precision Macromolecular Synthesis. *Chem. Rev.* **2016**, *116* (4), 2307–2413. doi.org/10.1021/acs.chemrev.5b00472.
(27) Zhao, H. Enzymatic Ring-Opening Polymerization (ROP) of Polylactones: Roles of Non-Aqueous Solvents. *Journal of Chemical Technology & Biotechnology* **2018**, *93* (1), 9–19. doi.org/10.1002/jctb.5444.
(28) Abedalwafa, M.; Wang, F.; Wang, L.; Li, C. Biodegradable Poly-epsilon-caprolactone (PCL) for tissue engineering applications: a review. 18.
(29) Poojari, Y.; Beemat, J. S.; Clarson, S. J. Enzymatic Synthesis of Poly(ε-Caprolactone): Thermal Properties, Recovery, and Reuse of Lipase B from Candida Antarctica Immobilized on Macroporous Acrylic Resin Particles. *Polymer Bulletin* **2013**, *70* (5), 1543–1552. doi.org/10.1007/s00289-013-0916-1.
(30) Polloni, A. E.; Veneral, J. G.; Rebelatto, E. A.; de Oliveira, D.; Oliveira, J. V.; Araújo, P. H. H.; Sayer, C. Enzymatic Ring Opening Polymerization of ω-Pentadecalactone Using Supercritical Carbon Dioxide. *The Journal of Supercritical Fluids* **2017**, *119*, 221–228. doi.org/10.1016/j.supflu.2016.09.019.
(31) Zhao, H.; Nathaniel, G. A.; Merenini, P. C. Enzymatic Ring-Opening Polymerization (ROP) of Lactides and Lactone in Ionic Liquids and Organic Solvents: Digging the Controlling Factors. *RSC Adv.* **2017**, *7* (77), 48639–48648. doi.org/10.1039/C7RA09038B.
(32) Pellis, A.; Comerford, J. W.; Weinberger, S.; Guebitz, G. M.; Clark, J. H.; Farmer, T. J. Enzymatic Synthesis of Lignin Derivable Pyridine Based Polyesters for the Substitution of Petroleum Derived Plastics. *Nature Communications* **2019**, *10* (1), 1762. doi.org/10.1038/s41467-019-09817-3.
(33) Rychlicka, M.; Gliszczyńska, A. Interesterification of Egg-Yolk Phosphatidylcholine with p-Methoxycinnamic Acid Catalyzed by Immobilized Lipase B from Candida Antarctica. *Catalysts* **2020**, *10* (10), 1181. doi.org/10.3390/catal10101181.
(34) Qian, X.; Wu, Q.; Xu, F.; Lin, X. Lipase-Catalyzed Synthesis of Polymeric Prodrugs of Nonsteroidal Anti-Inflammatory Drugs. *J. Appl. Polym. Sci.* **2013**, *128* (5), 3271–3279. doi.org/10.1002/app.38375.
(35) Toledo, M. V.; José, C.; Suster, C. R. L.; Collins, S. E.; Portela, R.; Bañares, M. A.; Briand, L. E. Catalytic and Molecular Insights of the Esterification of Ibuprofen and Ketoprofen with Glycerol. *Molecular Catalysis* **2021**, *513*, 111811. doi.org/10.1016/j.mcat.2021.111811.
(36) Kim, J. J.; Kim, H. K. Antioxidant and Antibacterial Activity of Caprylic Acid Vanillyl Ester Produced by Lipase-Mediated Transesterification. *J. Microbiol. Biotechnol.* **2021**, *31* (2), 317–326. doi.org/10.4014/jmb.2010.10018.
(37) Jung, H.J.; Song, Y. S.; Lim, C.J.; Park, E.H. Anti-Angiogenic, Anti-Inflammatory and Anti-Nociceptive Activities of Vanillyl Alcohol. *Arch. Pharm. Res.* **2008**, *31* (10), 1275–1279. doi.org/10.1007/s12272-001-2106-1.
(38) Lun Chung, H.; Zhi Hong, W.; Kuan Yu, L. Use of Vanillyl Alcohol for the Treatment of Parkinson's Disease. US20090258951A1. patents.google.com/patent/US20090258951A1/en.
(39) Zhu, Y.-J.; Zhou, H.-T.; Hu, Y.-H.; Tang, J.-Y.; Su, M.-X.; Guo, Y.-J.; Chen, Q.-X.; Liu, B. Antityrosinase and Antimicrobial Activities of 2-Phenylethanol, 2-Phenylacetaldehyde and 2-Phenylacetic Acid. *Food Chemistry* **2011**, *124* (1), 298–302. doi.org/10.1016/j.foodchem.2010.06.036.
(40) Liu, Y.; Zhao, Y.; Zhai, X.; Feng, X.; Wang, J.; Gong, P. Synthesis and Anti-Hepatitis B Virus Evaluation of Novel Ethyl 6-Hydroxyquinoline-3-Carboxylates in Vitro. *Bioorganic & Medicinal Chemistry* **2008**, *16* (13), 6522–6527. doi.org/10.1016/j.bmc.2008.05.029.
(41) Figueiredo, P. R.; Almeida, B. C.; Dourado, D. F. A. R.; Sousa, A. F.; Silvestre, A. J. D.; Carvalho, A. T. P. Enzymatic Synthesis of Poly(Caprolactone): A QM/MM Study. *ChemCatChem* **2020**, *12* (19), 4845–4852. doi.org/10.1002/cctc.202000780.
(42) Ashvar, C. S.; Devlin, F. J.; Bak, K. L.; Taylor, P. R.; Stephens, P. J. Ab Initio Calculation of Vibrational Absorption and Circular Dichroism Spectra: 6,8-Dioxabicyclo[3.2.1]Octane. *J. Phys. Chem.* **1996**, *100* (22), 9262–9270. doi.org/10.1021/jp953738p.
(43) Grimme, S.; Antony, J.; Ehrlich, S.; Krieg, H. A Consistent and Accurate Ab Initio Parametrization of Density Functional Dispersion Correction (DFT-D) for the 94 Elements H-Pu. *J. Chem. Phys.* **2010**, *132* (15), 154104. doi.org/10.1063/1.3382344.

(44) Zieniuk, B.; Groborz, K.; Wołoszynowska, M.; Ratusz, K.; Białecka-Florjańczyk, E.; Fabiszewska, A. Enzymatic Synthesis of Lipophilic Esters of Phenolic Compounds, Evaluation of Their Antioxidant Activity and Effect on the Oxidative Stability of Selected Oils. *Biomolecules* **2021**, *11* (2), 314. doi.org/10.3390/biom11020314.
(45) Marcilla, R.; de Geus, M.; Mecerreyes, D.; Duxbury, C. J.; Koning, C. E.; Heise, A. Enzymatic Polyester Synthesis in Ionic Liquids. *European Polymer Journal* **2006**, *42* (6), 1215–1221. doi.org/10.1016/j.eurpolymj.2005.12.021.
(46) Nguyen, H. T. H.; Short, G. N.; Qi, P.; Miller, S. A. Copolymerization of Lactones and Bioaromatics via Concurrent Ring-Opening Polymerization/Polycondensation. *Green Chem.* **2017**, *19* (8), 1877–1888. doi.org/10.1039/C6GC03238A.
(47) Gandini, A.; Silvestre, A. J. D.; Neto, C. P.; Sousa, A. F.; Gomes, M. The Furan Counterpart of Poly(Ethylene Terephthalate): An Alternative Material Based on Renewable Resources. *J. Polym. Sci. A Polym. Chem.* **2009**, *47* (1), 295–298. doi.org/10.1002/pola.23130.
(48) Pal, J.; Sanwaria, S.; Choudhary, A.; Thakur, K.; Nandan, B.; Srivastava, R. K. Thermally Initiated Trans-Esterification in Poly(ε-Caprolactone) and Its Dependence on Molecular Weight. *J Polym Environ* **2014**, *22* (4), 479–487. doi.org/10.1007/s10924-014-0669-4.
(49) Izunobi, J. U.; Higginbotham, C. L. Polymer Molecular Weight Analysis by ^{1}H NMR Spectroscopy. *J. Chem. Educ.* **2011**, *88* (8), 1098–1104. doi.org/10.1021/ed100461v.
(50) Ulker, C.; Gokalp, N.; Guvenilir, Y. Enzymatic Synthesis and Characterization of Polycaprolactone by Using Immobilized Lipase onto a Surface-Modified Renewable Carrier. *Polish Journal of Chemical Technology* **2016**, *18* (3), 134–140. doi.org/10.1515/pjct-2016-0060.
(51) Massoumi, B.; Ramezani, M.; Jaymand, M.; Ahmadinejad, M. Multi-Walled Carbon Nanotubes-g-[Poly(Ethylene Glycol)-b-Poly(ε-Caprolactone)]: Synthesis, Characterization, and Properties. *J Polym Res* **2015**, *22* (11), 214. doi.org/10.1007/s10965-015-0863-7.
(52) Almeida, B. C.; Figueiredo, P. R.; Dourado, D. F. A. R.; Paul, S.; Sousa, A. F.; Silvestre, A. J. D.; Quinn, D. J.; Moody, T. S.; Carvalho, A. T. P. Development of Enzymatic Variants for the Synthesis of Bioresorbable Polyesters. *Org. Process Res. Dev.* **2022**, *26* (8), 2351–2363. doi.org/10.1021/acs.oprd.1c00480.
(53) Stauch, B.; Fisher, S. J.; Cianci, M. Open and Closed States of Candida Antarctica Lipase B: Protonation and the Mechanism of Interfacial Activation. *J. Lipid Res.* **2015**, *56* (12), 2348–2358. doi.org/10.1194/jlr.M063388.
(54) Williams, C. J.; Headd, J. J.; Moriarty, N. W.; Prisant, M. G.; Videau, L. L.; Deis, L. N.; Verma, V.; Keedy, D. A.; Hintze, B. J.; Chen, V. B.; Jain, S.; Lewis, S. M.; Arendall, W. B.; Snoeyink, J.; Adams, P. D.; Lovell, S. C.; Richardson, J. S.; Richardson, D. C. MolProbity: More and Better Reference Data for Improved All-Atom Structure Validation. *Protein Science* **2018**, *27* (1), 293–315. doi.org/10.1002/pro.3330.
(55) Frisch, M. J.; Trucks, G. W.; Cheeseman, J. R.; Scalmani, G.; Caricato, M.; Hratchian, H. P.; Li, X.; Barone, V.; Bloino, J.; Zheng, G.; Vreven, T.; Montgomery, J. A.; Petersson, G. A.; Scuseria, G. E.; Schlegel, H. B.; Nakatsuji, H.; Izmaylov, A. F.; Martin, R. L.; Sonnenberg, J. L.; Peralta, J. E.; Heyd, J. J.; Brothers, E.; Ogliaro, F.; Bearpark, M.; Robb, M. A.; Mennucci, B.; Kudin, K. N.; Staroverov, V. N.; Kobayashi, R.; Normand, J.; Rendell, A.; Gomperts, R.; Zakrzewski, V. G.; Hada, M.; Ehara, M.; Toyota, K.; Fukuda, R.; Hasegawa, J.; Ishida, M.; Nakajima, T.; Honda, Y.; Kitao, O.; Nakai, H. Gaussian 09, Revision B.01. Gaussian 09, Revision B.01, Gaussian, Inc., Wallingford CT, 2009.
(56) Bayly, C. I.; Cieplak, P.; Cornell, W.; Kollman, P. A. A Well-Behaved Electrostatic Potential Based Method Using Charge Restraints for Deriving Atomic Charges: The RESP Model. *J. Phys. Chem.* **1993**, *97* (40), 10269–10280. doi.org/10.1021/j100142a004.
(57) Bianco, G.; Forli, S.; Goodsell, D. S.; Olson, A. J. Covalent Docking Using Autodock: Two-Point Attractor and Flexible Side Chain Methods: Covalent Docking with AutoDock. *Protein Science* **2016**, *25* (1), 295–301. doi.org/10.1002/pro.2733.
(58) Morris, G. M.; Huey, R.; Lindstrom, W.; Sanner, M. F.; Belew, R. K.; Goodsell, D. S.; Olson, A. J. AutoDock4 and AutoDockTools4: Automated Docking with Selective Receptor Flexibility. *Journal of Computational Chemistry* **2009**, *30* (16), 2785–2791. doi.org/10.1002/jcc.21256.
(59) Salomon-Ferrer, R.; Case, D. A.; Walker, R. C. An Overview of the Amber Biomolecular Simulation Package: Amber Biomolecular Simulation Package. *Wiley Interdisciplinary Reviews: Computational Molecular Science* **2013**, *3* (2), 198–210. doi.org/10.1002/wcms.1121.
(60) Maier, J. A.; Martinez, C.; Kasavajhala, K.; Wickstrom, L.; Hauser, K. E.; Simmerling, C. ff14SB: Improving the Accuracy of Protein Side Chain and Backbone Parameters from ff99SB. *J. Chem. Theory Comput.* **2015**, *11* (8), 3696–3713. doi.org/10.1021/acs.jctc.5b00255.

(61) Ryckaert, J.-P.; Ciccotti, G.; Berendsen, H. J. C. Numerical Integration of the Cartesian Equations of Motion of a System with Constraints: Molecular Dynamics of n-Alkanes. *Journal of Computational Physics* **1977**, *23* (3), 327–341. doi.org/10.1016/0021-9991(77)90098-5.
(62) Darden, T.; York, D.; Pedersen, L. Particle Mesh Ewald: An N·log(N) Method for Ewald Sums in Large Systems, 1998. doi.org/10.1063/1.464397.
(63) Warshel, A.; Levitt, M. Theoretical Studies of Enzymic Reactions: Dielectric, Electrostatic and Steric Stabilization of the Carbonium Ion in the Reaction of Lysozyme. *Journal of Molecular Biology* **1976**, *103* (2), 227–249. doi.org/10.1016/0022-2836(76)90311-9.
(64) Carvalho, A. T. P.; Barrozo, A.; Doron, D.; Kilshtain, A. V.; Major, D. T.; Kamerlin, S. C. L. Challenges in Computational Studies of Enzyme Structure, Function and Dynamics. *Journal of Molecular Graphics and Modelling* **2014**, *54*, 62–79. doi.org/10.1016/j.jmgm.2014.09.003.
(65) Torrie, G. M.; Valleau, J. P. Nonphysical Sampling Distributions in Monte Carlo Free-Energy Estimation: Umbrella Sampling. *Journal of Computational Physics* **1977**, *23* (2), 187–199. doi.org/10.1016/0021-9991(77)90121-8.
(66) Stewart, J. J. P. Optimization of Parameters for Semiempirical Methods V: Modification of NDDO Approximations and Application to 70 Elements. *J Mol Model* **2007**, *13* (12), 1173–1213. doi.org/10.1007/s00894-007-0233-4.
(67) Jindal, G.; Warshel, A. Exploring the Dependence of QM/MM Calculations of Enzyme Catalysis on the Size of the QM Region. *J. Phys. Chem. B* **2016**, *120* (37), 9913–9921. doi.org/10.1021/acs.jpcb.6b07203.
(68) Bakowies, D.; Thiel, W. Hybrid Models for Combined Quantum Mechanical and Molecular Mechanical Approaches. *J. Phys. Chem.* **1996**, *100* (25), 10580–10594. doi.org/10.1021/jp9536514.
(69) Nam, K.; Gao, J.; York, D. M. An Efficient Linear-Scaling Ewald Method for Long-Range Electrostatic Interactions in Combined QM/MM Calculations. *J. Chem. Theory Comput.* **2005**, *1* (1), 2–13. doi.org/10.1021/ct049941i.
(70) Kumar, S.; Rosenberg, J. M.; Bouzida, D.; Swendsen, R. H.; Kollman, P. A. THE Weighted Histogram Analysis Method for Free-Energy Calculations on Biomolecules. I. The Method. *Journal of Computational Chemistry* **1992**, *13* (8), 1011–1021. doi.org/10.1002/jcc.540130812.
(71) Grossfield, A. An Implementation of WHAM: The Weighted Histogram Analysis Method Version 2.0.9. **2018**, 18.
(72) Marcos-Alcalde, I.; Setoain, J.; Mendieta-Moreno, J. I.; Mendieta, J.; Gómez-Puertas, P. MEPSA: Minimum Energy Pathway Analysis for Energy Landscapes: Fig. 1. *Bioinformatics* **2015**, btv453. doi.org/10.1093/bioinformatics/btv453.
(73) Ruiz-Pernía, J. J.; Silla, E.; Tuñón, I.; Martí, S.; Moliner, V. Hybrid QM/MM Potentials of Mean Force with Interpolated Corrections. *J. Phys. Chem. B* **2004**, *108* (24), 8427–8433. doi.org/10.1021/jp049633g.
(74) Chuang, Y.-Y.; Corchado, J. C.; Truhlar, D. G. Mapped Interpolation Scheme for Single-Point Energy Corrections in Reaction Rate Calculations and a Critical Evaluation of Dual-Level Reaction Path Dynamics Methods. *J. Phys. Chem. A* **1999**, *103* (8), 1140–1149. doi.org/10.1021/jp9842493.
(75) Nguyen, K. A.; Rossi, I.; Truhlar, D. G. A Dual-level Shepard Interpolation Method for Generating Potential Energy Surfaces for Dynamics Calculations. *The Journal of Chemical Physics* **1995**, *103* (13), 5522–5530. doi.org/10.1063/1.470536.
(76) Neese, F.; Wennmohs, F.; Becker, U.; Riplinger, C. The ORCA Quantum Chemistry Program Package. *J. Chem. Phys.* **2020**, *152* (22), 224108. doi.org/10.1063/5.0004608.